All-electronic terahertz spectroscopy system with terahertz free-space pulses

J. S. Bostak,* D. W. van der Weide,† D. M. Bloom, and B. A. Auld

E. L. Ginzton Laboratory, Stanford University, Stanford, California 94305

E. Özbay

Ames Laboratory and the Microelectrics Research Center, Iowa State University, Ames, Iowa 50011

Received January 27, 1994; revised manuscript received April 20, 1994

We have developed all-electronic integrated circuits that generate and detect picosecond pulses. We have used these circuits with integrated antennas in a system capable of free-space spectroscopy in the terahertz regime. With this system we have measured magnitude- and phase-transmission characteristics for a variety of samples in the frequency range of 200 GHz–1 THz.

1. INTRODUCTION

In the study and the application of picosecond electromagnetic pulse propagation, the generation and the detection of these pulses is usually done with ultrashort optical pulses driving photoconductive switches that are used as both transient generators and samplers.[1,2] These systems have been applied to problems in terahertz (THz) spectroscopy.[3–8] Fourier analysis of the detected pulses, with and without a test sample in the beam path, yields the magnitude and the phase of the transmission of the sample as a function of frequency. In contrast to this hybrid optical–electronic approach, we have developed an all-electronic system that uses monolithic nonlinear transmission lines (NLTL's) as ultrafast voltage step generators for both generating picosecond pulses and driving monolithically integrated diode samplers for the detection of these pulses. The advantages of this approach lie in its relative simplicity and its robustness. Recently, similar all-electronic systems have been applied to THz spectroscopy but have been limited to frequencies below 250 GHz.[9] We have used our system to perform spectroscopic measurements from 250 to 375 GHz with 2-dB accuracy over a 20-dB dynamic range. We have also demonstrated measurements from 200 GHz to 1 THz with a signal-to-noise (S/N) ratio of 40 and 10 dB at the low and the high ends of the band, respectively.

2. NONLINEAR TRANSMISSION LINES

Nonlinear transmission lines are synthetic structures of series inductors (approximated by sections of a high-impedance transmission line) with varactor diodes periodically placed as shunt elements. On this structure a voltage shock wave develops from a sinusoidal input because the propagation velocity varies with the nonlinear capacitance–voltage relationship of the diodes, $v_p = 1/[LC_{tot}(V)]^{1/2}$, where L is the inductance and $C_{tot}(V)$ is the sum of the varactor capacitance and the parasitic capacitance of the line, all per unit length. Limitations of the NTLT arise from its periodic cutoff frequency, $\omega_{per} = 2/[LC_{tot}(V)]^{1/2}$, waveguide dispersion, interconnect metallization losses, and diode resistive losses.

3. GENERATION AND DETECTION OF PICOSECOND PULSES

We have previously reported NLTL's that produce 1-V, 1.8-ps fall-time shock-wave outputs at 300 K (Ref. 10) and 3.5-V, 880-fs fall-time shock-wave outputs at 77 K.[11] In the experiments described in this paper we applied the ultrafast-pulse-generating capability of these NLTL's to drive antennas and a sampler in a coherent, all-electronic free-space signal generation and detection system similar to that described in previous studies.[10–12] A summary of the important features as well as some modifications that were made to improve the performance in a spectroscopy system application are given below.

We used NLTL's integrated with magnetic dipole (slot) antennas measuring 5 μm wide and 190 μm long to realize a free-space picosecond-pulse generator integrated circuit (IC). High-resistivity (10 kΩ cm) silicon hyperhemispheres[13] were used to collect and to focus the quasi-optical beam. Off-axis paraboloidal mirrors collimated and redirected the beam onto a detector chip. The detector IC consisted of an all-electronic two-diode sampler[14] whose radio-frequency (RF) port was driven by a slot antenna identical to that used in the generator IC and whose local-oscillator (LO) port was driven by a NLTL. The generator and the detector were each driven by synthesized microwave-signal generators and microwave amplifiers capable of producing a +30-dBm, 5–10-GHz microwave signal. The two signal generators were phase locked and were offset in frequency by an intermediate frequency (IF) from 0.5 to 10 Hz. A portion of each signal was fed to a mixer to provide a trigger signal to an audio-frequency spectrum analyzer that was connected to the IF port of the detector. Previous experiments used a signal microwave-signal generator and mechanical frequency shifter to drive the generator and

0740-3224/94/122561-05$06.00

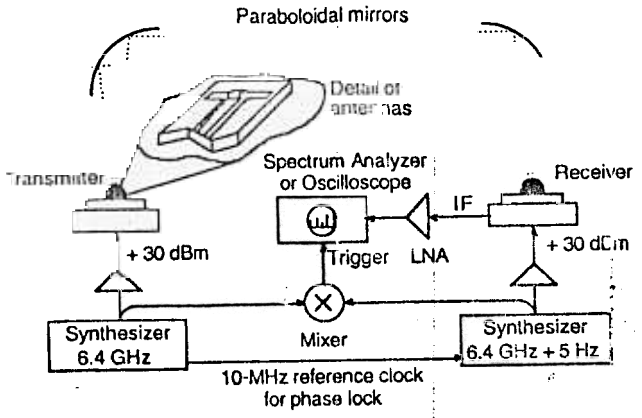

Fig. 1. Experimental setup. IF, intermediate frequency; LNA, low-noise amplifier.

the detector.[10,11] The use of two phase-locked microwave synthesizers eliminated the distortion caused by the mechanical frequency shifter.

The complete system is shown in Fig. 1. Because of the difficulty in maintaining a stable 77-K environment for performing spectroscopic measurements, only 30 I-K NLTL's were used in the experiments reported in this paper. We have previously shown that a received pulse, generated and detected at 77 K, contains spectral content from 5 GHz to 3 THz (Ref. 11); the 300-K pulses provide useful spectral content to as high as approximately 1 THz.

4. FREE-SPACE SPECTROSCOPY SYSTEM

A. System Description

To perform a free-space spectroscopic measurement, a sample under test can be placed in the THz beam. By finding the ratio of the detected signal spectrum with and without the sample in place, one can obtain the transmission of the sample as a function of frequency. Because the system detects voltage, not power, both the magnitude and the phase of the transmission can be obtained.

Subsection 4.B describes free-space spectroscopic measurements on five separate samples. The first sample is a multiple-bandpass filter, or a Fabry–Perot étalon, produced by the Center for Submillimeter Radiophysics, St. Petersburg, Russia, and obtained through the cooperation of the Max-Planck-Institut für Festkörperforschung, Stuttgart, Germany. The second sample is a sheet of Plexiglas brand of acrylic sheet, manufactured by the Rohm & Haas Corporation, Philadelphia, Pennsylvania. The third through fifth samples are examples of photonic band-gap structures, fabricated by E. Özbay at Iowa State University, Ames, Iowa.

B. Experiments

1. *Fabry–Perot Étalon*

In the first experiment the sample under test was a multiple-bandpass filter. Because the filter was small, it was placed close to the generator, where the beam diameter is smallest. The disadvantage of placing the sample close to the generator as opposed to between the two off-axis paraboloidal mirrors is that the beam is diverging and hence is not a true plane wave.[15] Only the center of the beam indicated by the dotted lines in Fig. 1 would arrive at normal incidence to the sample. The edges of the beam deviate the most from normal incidence and strike the sample at 14° from the normal in the case of this experiment. This nonideality was one source of measurement error in the experiment.

The manufacturer of the filter[16] had used a backward-wave oscillator spectrometer to characterize the magnitude of the filter transmission from 235 to 390 GHz. The filter's passbands were measured by the manufacturer to be centered near 279 and 348 GHz. Our first goal was to characterize the filter in the 235–390-GHz region as the manufacturer had done, and our second goal was to characterize the filter at still higher frequencies to as high as the THz regime.

A comparison of the manufacturer's measurement with ours is shown in Fig. 2. Compared with the data provided by the manufacturer, our data are accurate within 2 dB over a 20-dB dynamic range from −7- to −27-dB transmittance. Below −27-dB transmittance our system was not capable of accurately reproducing the manufacturer's data. We can attribute this limitation to a lower S/N ratio in our system. The noise floor was shown to be set largely by the noise of the local oscillator.[17] The sampling bridge in the detector IC used in these experiments was not well balanced with respect to the local oscillator, and some of the relatively large-amplitude local-oscillator signal was superimposed on the small-amplitude detected THz signal. To decrease the noise floor, sampling bridges that are properly balanced with respect to the local oscillator should be used.

A second way to decrease the noise floor is to reduce the effects of phase noise on the measurement results. This reduction can be accomplished by use of synthesizers with less phase noise. The effect of the phase noise from the two phase-locked synthesizers was calculated to be equivalent to 740-fs worst-case rms jitter in the time domain. This jitter limits our ability to measure subpicosecond signals accurately. As an alternative to the use of synthesizers with less phase noise, the IF could be increased so that the downconverted harmonics are spaced farther apart in frequency and are less susceptible to the phase noise from other harmonics.

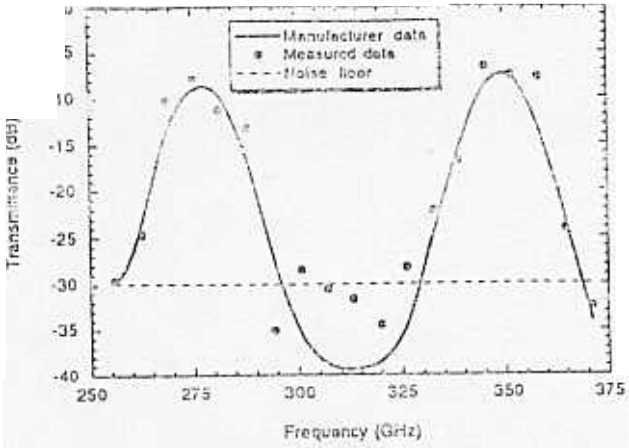

Fig. 2. Manufacturer data and measured data for submillimeter-wave filter.

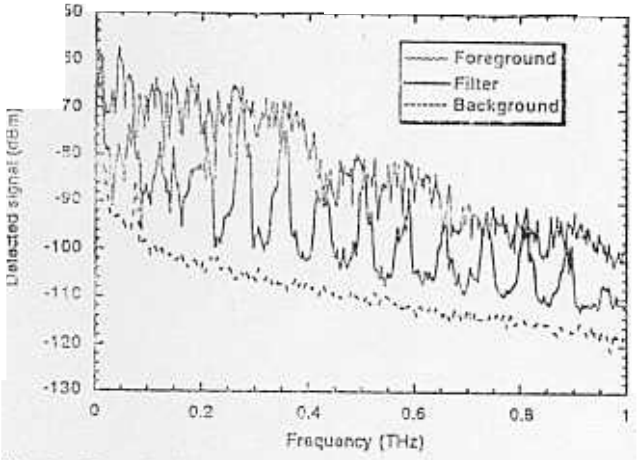

Fig. 3. Extended-frequency-range measured data for submillimeter-wave filter. Upper curve, foreground; middle curve, filter; lower curve, background.

We can also increase the S/N ratio by increasing the signal level in the system. One way to increase the signal level is to use broadband antennas. The magnetic dipole antennas currently used are resonant antennas and have a radiation resistance that is a strong function of frequency.

Figure 3 shows data from a measurement that spans the frequency range from 6.4 GHz to 1 THz. Here we plot separately the foreground (detected signal with no filter in place), the radiation with the filter in place, and the background (detected signal with beam blocked). The upper trace, which represents the foreground radiation, shows a monotonically decreasing frequency spectrum that is typical of measurements made with this system. The middle trace, which represents the filter measurement, shows clearly visible transmission peaks out to 1 THz. This periodic repetition of the signal peaks verifies that the filter is indeed an étalon and not simply a bandpass filter. If S/N ratio is calculated as the ratio of the foreground signal to the background signal, the S/N ratio is seen to be at least 20 dB over the entire frequency range from 6.4 GHz to 1 THz. A more conservative estimate, which accounts for the effects of phase noise between the two synthesizers, however, is the ratio of detected passband to stop band in the filter signal. Still, with this definition the S/N ratio is at least 10 dB over the entire frequency range.

2. *Plexiglas Sheet*

Whereas the previous experiment with the Fabry–Perot étalon demonstrated the magnitude transfer function of the étalon, the purpose of this experiment was to demonstrate the phase transmission through a sheet of Plexiglas. In this case the Plexiglas sheet was large enough that it could be placed between the two off-axis paraboloidal mirrors. The collimated beam was then normally incident upon the sheet at all points. The approach that is taken is similar to that of the previous experiment. A simplified explanation, which is elaborated on below, is as follows. A ratio is taken of the detected signal spectrum with and without the Plexiglas sheet in place. The phase of this signal spectrum indicates the relative phase delay imposed by Plexiglas as a function of frequency.

In this experiment we are interested in the phase transmission through the bulk material Plexiglas; we are not interested in the effects of the reflections at the air–Plexiglas interface. The effects of single reflections at the interface can be removed by measurement of the signal spectra $\tilde{A}_1(f)$ and $\tilde{A}_2(f)$ through two different sheets of Plexiglas of thicknesses l_1 and l_2,[15] respectively: because the THz beam experiences the same single reflections at both sheets, dividing $\tilde{A}_2(f)$ by $\tilde{A}_1(f)$ gives the effect of propagation through material of thickness $l_2 - l_1$. That is, if

$$\tilde{A}_1(f) = A_1(f)\exp[-j\Phi_1(f)],$$
$$\tilde{A}_2(f) = A_2(f)\exp[-j\Phi_2(f)],$$

then

$$\tilde{H}_{l_2-l_1}(f) = \frac{\tilde{A}_2(f)}{\tilde{A}_1(f)} \tag{1}$$
$$= \frac{A_2(f)}{A_1(f)} \exp\{-j[\Phi_2(f) - \Phi_1(f)]\} \tag{2}$$

gives the effect of propagation through material of thickness $l_2 - l_1$.

The effects of multiple reflections are more difficult to remove. Arjavalingam *et al.*[15] selected Plexiglas thicknesses such that multiple reflected pulses arrive at the receiver well after the main pulse. The unwanted pulses can then be removed by limitation of the time window of the measurement. Unfortunately, for the thicknesses of Plexiglas and the pulse-repetition rates available to us, the double-pass transit time for even the lowest-order (doubly) reflected pulse was longer than the period of the pulse-repetition rate, thus making removal of the unwanted pulse by time-windowing impossible. Nonetheless, we did not see significant effects of this pulse in the measurement data.

Figure 4 shows the value $\Phi = \Phi_2 - \Phi_1$ plotted as a function of frequency from 250 to 370 GHz after propagation through two sheets of Plexiglas with $l_2 = 9.36$ mm and $l_1 = 6.35$ mm, respectively. A line is also fitted to the

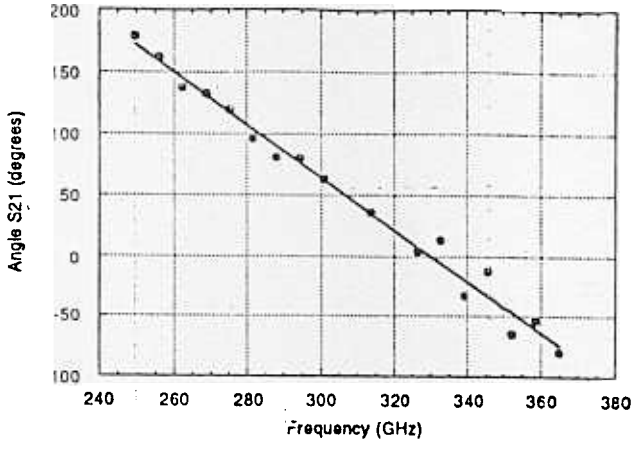

Fig. 4. Phase difference between transmission through two Plexiglas sheets. One sheet is 3 mm thicker than the other.

data points. The average refractive index of the Plexiglas in this frequency range can then be calculated from the formula[15]

$$n = 1 + \frac{1}{360^\circ}\frac{\Delta\Phi}{\Delta f}\frac{c_0}{(l_2 - l_1)} \tag{3}$$

$$= 1 + \frac{1}{360^\circ}\frac{2.1773^\circ}{10^9\ \mathrm{s}^{-1}}\frac{3 \times 10^8\ \mathrm{m/s}}{3.01 \times 10^{-3}\ \mathrm{m}} \tag{4}$$

$$= 1.603, \tag{5}$$

where the expression $(2.1773^\circ/10^9\ \mathrm{s}^{-1})$ is the slope of the fitted line in Fig. 4. The resultant index of Plexiglas, $n = 1.603$, is within 1% of the published values $n = 1.61 \pm 0.01$ and $n = 1.62 \pm 0.01$ at 142.86 and 344.83 GHz, respectively, obtained with the open-resonator method of Fourier-transform spectroscopy.[18]

3. *Photonic Band-Gap Structures*

The final set of experiments concerns magnitude-transmission measurements on photonic band-gap structures. A photonic bandgap structure is a large-scale model of an atomic lattice that supports a finite set of propagating modes of electromagnetic radiation, much as an atomic lattice supports only a finite set of allowable electron energies. These structures are currently being considered for use as microcavities in single-mode light-emitting diode applications.[19] Recently, photonic band-gap structures with interesting stop-band characteristics in the 5–150-GHz regime were fabricated and were measured.[20] However, photonic band-gap structures with stop bands in the 100–500-GHz regime are now available.[21–23] Limited measurement tools exist for measuring the magnitude transfer characteristics of these submillimeter-wave photonic band-gap structures. The purpose of these experiments was to measure their magnitude characteristics and to compare the data with theoretically predicted results.

As in the first experiment involving the Fabry–Perot étalon, the structures were small, so they were placed close to the generator where the beam diameter was smallest. Figures 5–7 show the measured magnitude transmission through photonic band-gap structures with theoretical stop bands in the ranges of 130–180 GHz, 230–380 GHz, and 340–510 GHz, respectively. The fluctuations in the data in the passband are due in part to the limited accuracy of the measurements and in part to the nonunity transmission coefficient across the passband. Because analytical techniques for calculating the transmission coefficient of the photonic band-gap structures are not yet fully developed, there is currently no way to distinguish the effects of measurement inaccuracy and variation in the transmission coefficient in the passband.

Comparing the stop bands in the figures with the theoretical stop bands leads to several interesting conclusions. First, in all cases the measured stop bands agree with the theoretical stop bands within 15%. This much discrepancy is attributed to one of two causes: First, the accuracy of the theoretical calculations is not guaranteed because the science of photonic band gaps is relatively new. Second, the stop-band edges change as a function of the incident angle of the electromagnetic radiation, much as the band gap of a semiconductor lattice changes with position in the Brillouin zone. Some misalignment of the photonic band-gap structure in the THz beam path, or the fact that the THz beam is not quite a plane wave, gives some degree of ambiguity to the angle of the incident THz radiation.

The second conclusion that can be drawn is that, assuming that the depth of the stop band (in decibels) is the same for each structure, the measurement dynamic range

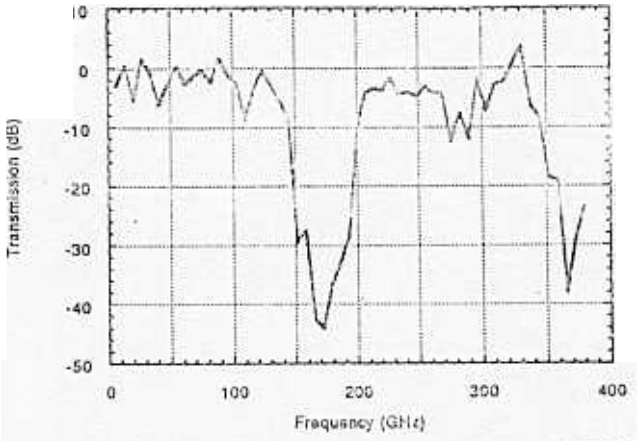

Fig. 5. Measured magnitude transmission for 130–180-GHz photonic band-gap structure.

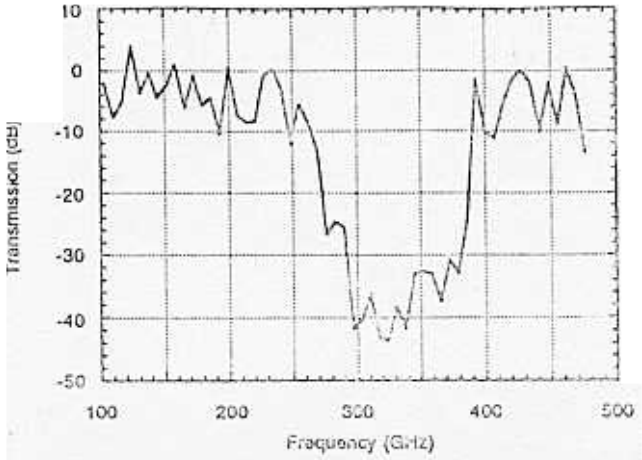

Fig. 6. Measured magnitude transmission for 230–380-GHz photonic band-gap structure.

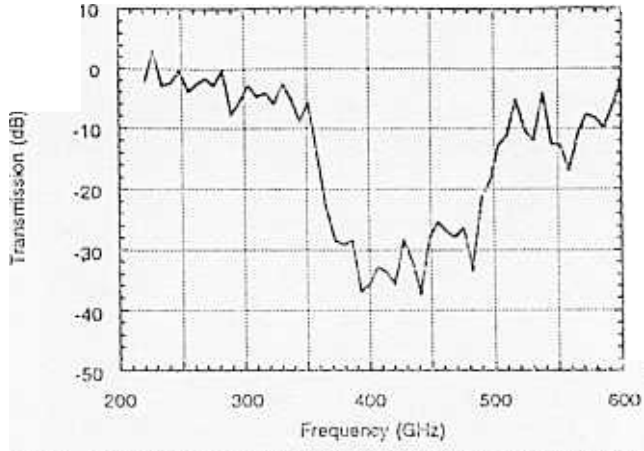

Fig. 7. Measured magnitude transmission for 340–510-GHz photonic band-gap structure.

of our THz measurement system is a maximum, approximately 40 dB, in the 130–180-GHz range. The measurement dynamic range decreases to approximately 35 and 30 dB in the 230–380-GHz and the 340–510-GHz ranges, respectively. This decrease in dynamic range is precisely what would be predicted by the decreasing strength of the detected THz signal as a function of frequency, which we reported previously.[11,17]

5. CONCLUSIONS

In conclusion, we have developed all-electronic integrated circuits that generate and detect picosecond pulses. We have used these circuits with integrated antennas in a system capable of free-space spectroscopy in the terahertz regime. With this system we have measured magnitude- and phase-transmission characteristics for a variety of samples in the frequency range of 200 GHz–1 THz. We have used our system to perform spectroscopic measurements from 250 to 375 GHz with 2-dB accuracy over a 20-dB dynamic range. We have also demonstrated measurements from 200 GHz to 1 THz with a signal-to-noise ratio of 40 and 10 dB at the low and the high ends of the band, respectively.

ACKNOWLEDGMENTS

This research was supported by the Joint Services Electronics Program under contract N00014-92-J-1050. J. S. Bostak acknowledges a Joint Services Electronics Program fellowship. The authors thank J. Martin and P. Prather for circuit assembly and acknowledge discussions with M. J. W. Rodwell and M. T. Kauffman. Thanks are due to Watkins-Johnson Company for loans of equipment.

*Present address, Vitesse Semiconductor Corporation, Sunnyvale, California 94086.

†Present address, Max-Planck-Institut für Festkörperforschung, D-70569 Stuttgart, Germany.

REFERENCES

1. P. R. Smith, D. H. Auston, and M. C. Nuss, "Subpicosecond photoconducting dipole antennas," IEEE J. Quantum Electron. 24, 255–260 (1988).
2. C. Fattinger and D. Grischkowsky, "Terahertz beams," Appl. Phys. Lett. 54, 490–492 (1989).
3. M. van Exter, "Terahertz time-domain spectroscopy of water vapor," Opt. Lett. 14, 1128–1130 (1989).
4. M. van Exter and D. Grischkowsky, "Optical and electronic properties of doped silicon from 0.1 to 2 THz," Appl. Phys. Lett. 56, 1694–1696 (1990).
5. D. Grischkowsky, S. Keiding, M. van Exter, and C. Fattinger, "Far-infrared time-domain spectroscopy with terahertz beams of dielectric and semiconductors," J. Opt. Soc. Am. B 7, 2006–2015 (1990).
6. J. E. Pedersen and S. R. Keiding, "THz time-domain spectroscopy of nonpolar liquids," IEEE J. Quantum Electron. 28, 2518–2522 (1992).
7. M. C. Nuss, P. M. Mankiewich, M. L. O'Malley, E. H. Westerwick, and P. B. Littlewood, "Dynamic conductivity and 'coherence peak' in $YBa_2Cu_3O_7$ superconductors," Phys. Rev. Lett. 66, 3305–3308 (1991).
8. M. C. Nuss, K. W. Goossen, J. P. Gordon, P. M. Mankiewich, M. L. O'Malley, and M. Bhusan, "Terahertz time-domain measurement of the conductivity and superconducting band gap in niobium," J. Appl. Phys. 70, 2238–2241 (1991).
9. Y. Konishi, M. Kamegawa, M. Case, R. Yu, M. J. W. Rodwell and R. A. York, "Picosecond electrical spectroscopy using monolithic GaAs circuits," Appl. Phys. Lett. 61, 2829–283 (1992).
10. D. W. van der Weide, J. S. Bostak, B. A. Auld, and D. M Bloom, "All-electronic free-space picosecond pulse generation and detection," Electron. Lett. 27, 1412–1413 (1991).
11. D. W. van der Weide, J. S. Bostak, B. A. Auld, and D. M Bloom, "All-electronic generation of 880 fs, 3.5 V shockwaves and their application to a 3 THz free-space signal generation system," Appl. Phys. Lett. 62, 22–24 (1993).
12. M. Kamegawa, Y. Konishi, M. Case, R. Yu, and M. J. W Rodwell, "Coherent, broadband millimeter-wave spectroscopy using monolithic GaAs circuits," in *Optical Millimeter-Wave Interactions: Measurement, Generation Transmission and Control* (Institute of Electrical and Electronics Engineers, New York, 1991).
13. N. Katzenellenbogen and D. Grischkowsky, "Efficient generation of 380 fs pulses of THz radiation by ultrafast laser pulse excitation of a biased metal-semiconductor interface," Appl. Phys. Lett. 58, 222–224 (1991).
14. R. A. Marsland, C. J. Madden, D. W. Van Der Weide, M. S. Shakouri, and D. M. Bloom, "Monolithic integrated circuits for mm-wave instrumentation," in *IEEE GaAs IC Symposium Technical Digest* (Institute of Electrical and Electronics Engineers, New York, 1990), Vol. 19, pp. 19–22.
15. G. Arjavalingam, Y. Pastol, J. Halbout, and G. V. Kopcsay, "Broad-band microwave measurements with transient radiation from optoelectronically pulsed antennas," IEEE Trans. Microwave Theory Tech. 38, 615–621 (1990).
16. Center for Submillimeter Radiophysics, St. Petersburg, Russia, in cooperation with the Max-Planck-Institut für Festkörperforschung, Stuttgart, West Germany.
17. J. S. Bostak, "All electronic generation and detection of free-space terahertz radiation with applications to free-space terahertz spectroscopy," Ph.D. dissertation (Stanford University, Stanford, Calif., 1994).
18. M. N. Afsar, "Dielectric measurement of millimeter-wave materials," IEEE Trans. Microwave Theory Tech. MTT-32, 1598–1609 (1984).
19. E. Yablonivich, "Photonic band-gap structures," J. Opt. Soc. Am. B 10, 283–295 (1993).
20. W. M. Robertson, G. Arjavalingam, R. D. Meade, K. D. Brommer, A. M. Rappe, and J. D. Joannopoulos, "Measurement of photonic band structure in a two-dimensional periodic dielectric array," Phys. Rev. Lett. 68, 2023–2026 (1992).
21. E. Özbay, E. Michel, G. Tuttle, R. Biswas, M. Sigalas, and K. M. Ho, "Micromachined millimeter-wave photonic bandgap crystals," Appl. Phys. Lett. 64, 2059–2061 (1994).
22. E. Özbay, E. Michel, G. Tuttle, R. Biswas, K. M. Ho J. Bostak, and D. M. Bloom, "Terahertz spectroscopy of three-dimensional photonic band-gap crystals," Opt. Lett. 19, 1155–1157 (1994)
23. E. Özbay, G. Tuttle, R. Biswas, K. M. Ho, J. Bostak, and D. M. Bloom, "New double-etch geometry for millimeter-wave photonic crystals with a semi-tunable photonic band gap," Appl. Phys. Lett. 66, 1446 (1994).